Phys. Lett. B 855 (2024) 138850

Contents lists available at ScienceDirect

Physics Letters B

journal homepage: www.elsevier.com/locate/physletb

Letter

# Multiple chiral doublet bands in $^{104}$Rh

A. Krakó [a,b], D. Sohler [a,*], J. Timár [a], I. Kuti [a], Q.B. Chen [c], S.Q. Zhang [d], J. Meng [d], K. Starosta [e], T. Koike [f], E.S. Paul [g], D.B. Fossan [h,1], C. Vaman [h]

[a] HUN-REN Institute for Nuclear Research, ATOMKI, Pf. 51, 4001 Debrecen, Hungary
[b] University of Debrecen, Doctoral School of Physics, 4032 Debrecen, Egyetem tér 1, Hungary
[c] Department of Physics, East China Normal University, Shanghai 200241, China
[d] School of Physics and State Key Laboratory of Nuclear Physics and Technology, Peking University, Beijing 100871, China
[e] Department of Chemistry, Simon Fraser University, Burnaby, British Columbia V5A 1S6, Canada
[f] Department of Physics, Tohoku University, Sendai 980-8578, Japan
[g] Department of Physics, University of Liverpool, Liverpool L69 7ZE, United Kingdom
[h] Department of Physics and Astronomy, State University of New York, Stony Brook, NY, 11794-3800, USA

ARTICLE INFO

Editor: B. Blank

ABSTRACT

Two new negative-parity bands have been identified in the odd-odd $^{104}$Rh nucleus. According to their experimentally observed properties, they have the same $\pi(1g_{9/2})^{-1}\otimes\nu(1h_{11/2})^{1}$ high-$j$ configuration as the previously known negative-parity chiral doublet bands. This observation raises the possibility of the existence of multiple chiral doublet bands, M$\chi$D, in this nucleus. Comparing the properties of the observed bands with results of detailed theoretical calculations, one can conclude that the lower energy parts of bands 1 and 2 are chiral partner bands with the $\pi(1g_{9/2})^{-1}\otimes\nu(1h_{11/2})^{1}$ two-quasiparticle configuration, while bands 3 and 4 are chiral partner bands with the $\pi(1g_{9/2})^{-1}\otimes\nu(1g_{7/2})^{-2}(1h_{11/2})^{1}$ four-quasiparticle configuration. Thus, M$\chi$D based on different configurations is observed in $^{104}$Rh.

## 1. Introduction

Chiral rotation of triaxial nuclei when, in the intrinsic frame of the rotating triaxial nucleus, the total angular momentum vector lies outside the three principal planes, was proposed in 1997 [1] as a novel form of spontaneous symmetry breaking. After the first identification of the phenomenon in four $N = 75$ isotones in 2001 [2], many chiral candidate nuclei have been reported experimentally in the $A \sim 80$, 100, 130, and 190 mass regions [3–22]. A review of the experimentally observed chiral bands can be found in Ref. [23]. Observation of chiral bands also in odd-mass nuclei [10,18,19] emphasizes the importance of the triaxial core [19], while comparison of their properties with those of the odd-odd cases suggests that in the chirality regions chiral geometry can be robust against the change of configuration. This raises the possibility of having more than one chiral doublet structures in a single nucleus with different configurations. Indeed, it was demonstrated by Meng et al. [24–27], based on adiabatic and configuration-fixed constrained triaxial covariant density functional theory (CDFT) calculations, that it is possible to have multiple pairs of chiral doublet bands in a single nucleus. They introduced the acronym M$\chi$D for this phenomenon. The first experimental evidence for the predicted M$\chi$D with different and with identical configurations have been reported in $^{133}$Ce [28] and in $^{103}$Rh [29], respectively. Since then, the M$\chi$D phenomenon has been observed in several odd-mass nuclei, as well as in some odd-odd (i.e. $^{78}$Br [22]) and even-even (i.e. $^{136}$Nd [30]) nuclei. However, in the $A \sim 100$ mass region it has only been reported in odd-mass nuclei.

In this Letter we report on the observation of two new negative-parity bands in $^{104}$Rh, which have similar properties to the previously observed chiral bands [14], and which are interpreted also as a chiral band pair. This observation exhibits the existence of M$\chi$D in this odd-odd nucleus for the first time in the $A \sim 100$ mass region.

## 2. Experimental methods and results

Medium- and high-spin states of $^{104}$Rh were populated using the $^{96}$Zr($^{11}$B,3n) reaction at a beam energy of 40 MeV. The beam, provided by the 88-inch Cyclotron of the Lawrence Berkeley National Laboratory (LBNL), impinged upon an enriched 500 μg/cm$^2$ thick self-supporting Zr

* Corresponding author.
*E-mail address:* sohler@atomki.hu (D. Sohler).
[1] Deceased.

https://doi.org/10.1016/j.physletb.2024.138850
Received 15 December 2023; Received in revised form 19 June 2024; Accepted 1 July 2024
Available online 6 July 2024

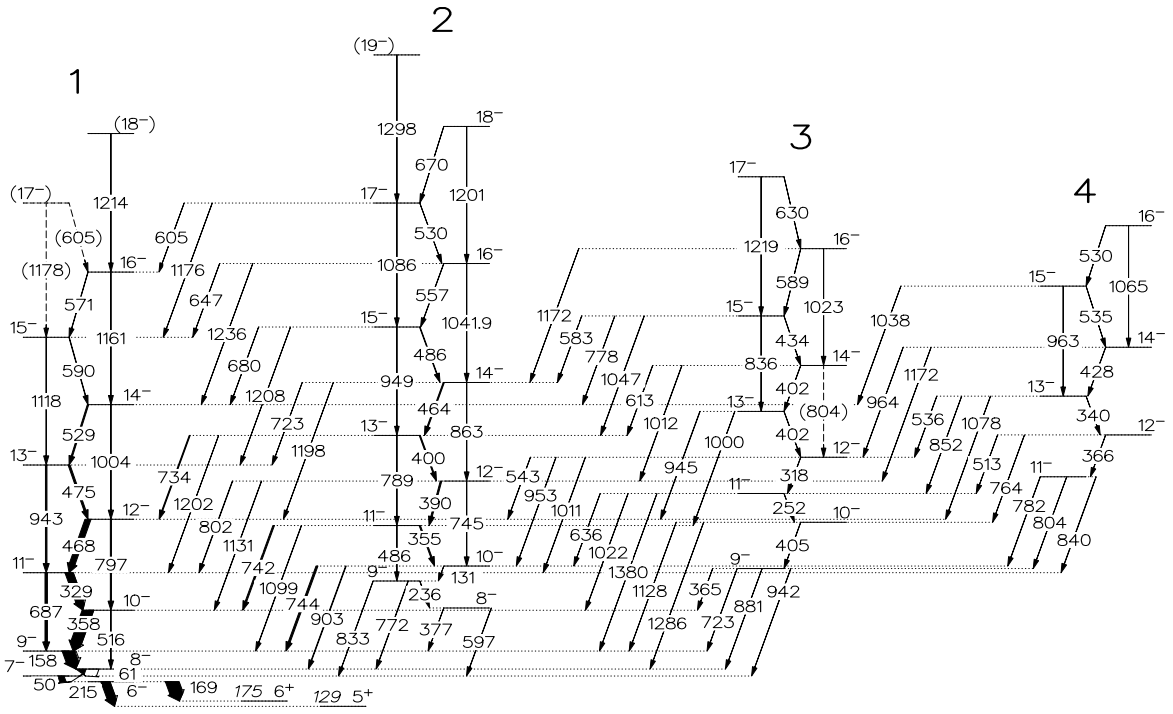


**Fig. 1.** Partial level scheme of $^{104}$Rh. The energies are given in keV, the widths of the arrows are proportional to the relative transition intensities.

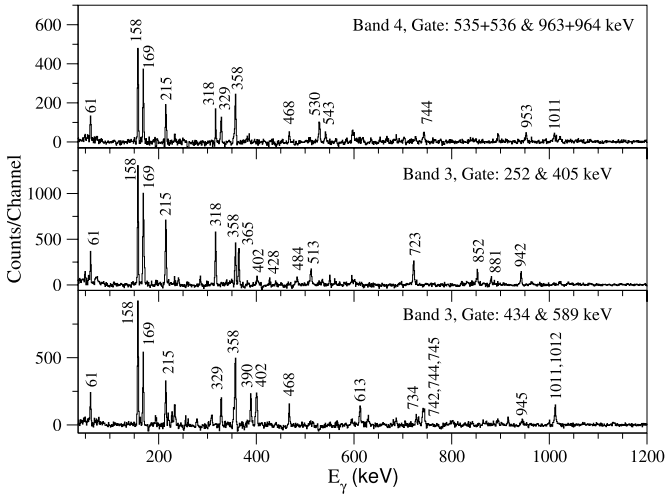


**Fig. 2.** Typical $\gamma\gamma\gamma$-coincidence spectra obtained in the present work showing the placement of the $\gamma$ rays in bands 3 and 4.

foil. The emitted $\gamma$-rays were detected by the Gammasphere spectrometer. [31,32] Approximately $9 \times 10^8$ four- and higher-fold events were accumulated and sorted off-line into 2-d and 3-d histograms. The data analysis was carried out using the RADWARE software package [33]. A more complete level scheme of $^{104}$Rh was constructed using the observed coincidence relations, as well as energy and intensity balances of the gamma transitions. Spin and parity assignments for the new states were deduced from the measurements of angular-intensity ratios, based on the method of directional correlation from oriented states (DCO) [34].

Results of the first analysis of the collected data set have been published in Ref. [14]. A chiral band pair with the $\pi g_{9/2} \otimes \nu h_{11/2}$ configuration has been reported. That analysis concentrated only on the published band pair. A more extensive analysis of the data set has been performed in this work, which provided an extended level scheme with several new bands. In this Letter we concentrate on the negative-parity bands and on the possible multiple chiral doublets among them. Two new negative-parity medium-spin rotational bands have been found. A partial level scheme showing the bands relevant to the focus of this Letter is plotted in Fig. 1. Bands 1 and 2 are the formerly reported chiral band pair [14], while bands 3 and 4 are the newly identified bands. Most of the previously published levels and transitions have been confirmed and bands 1 and 2 have been extended by 1 and 2 levels, respectively. The published placement and decay of the $17^-$ member of band 1 could not be unambiguously confirmed, as the energies of the depopulating transitions overlap with that of depopulating the $17^-$ member of band 2. They cannot be separated from coincidence relations with transitions below them in the level scheme. In case of band 2, these transitions are in coincidence with the 1298 keV transition above the $17^-$ level. However, in case of band 1 no transition populating the $17^-$ level could be found. Bands 3 and 4 could be firmly placed by the coincidence relations of the many transitions connecting them to each other and to bands 1 and 2. Typical $\gamma\gamma\gamma$-coincidence spectra supporting the placements of the new bands are seen in Fig. 2. Dipole or quadrupole character could be determined from the measured DCO ratios for many new transitions. The measured DCO ratio values for the $\Delta I = 1$ transitions matched with the values expected for pure dipole transitions (~0.6) within the experimental errors. Thus, we accepted pure M1 multipolarity for them. The derived characters assisted in spin-parity determinations for the new levels. The parities were deduced using the additional assumption that if a level decays by both quadrupole and dipole transitions with comparable intensities, then the quadrupole transition is E2. The 953, 1000, 1012 and 1047 keV transitions from band 3 to band 2 have been found to have E2 character, fixing the spin-parities of the levels in the upper part of band 3, as they are shown in Fig. 1. The spin-parities of the levels in the lower part of band 3 are derived from the observed dipole character of 252, 318, 402 keV transitions, and from the many linking transitions to the different spin-parity levels of bands 1 and 2. The spin-parities of the levels in band 4 could be derived from the obtained E2 character of the 804 keV and the 1172 keV decay-out transitions. These spin-parities are confirmed by the obtained dipole character of the 1078 keV and 1038 keV transitions.

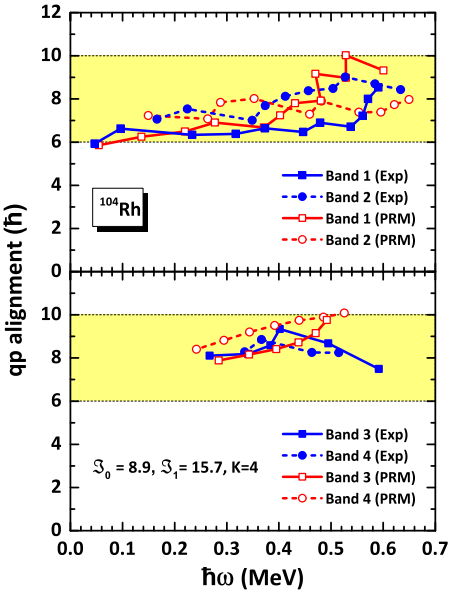


**Fig. 3.** Comparisons between the experimental and theoretical quasiparticle alignments of bands 1, 2, 3, and 4.

## 3. Discussion

To assist in the configuration assignments for bands 1-4, we have derived their quasiparticle alignments as defined in Ref. [35] (see in Fig. 3) and the in-band $B(M1)/B(E2)$ ratios of reduced transition probabilities (see in Fig. 5). The intrinsic quantum number $K = 4$ and the $\mathcal{J}_0 = 8.9\ \hbar^2/\text{MeV}$ and $\mathcal{J}_1 = 15.7\ \hbar^4/\text{MeV}^3$ parameters of the Harris formula $\mathcal{J} = \mathcal{J}_0 + \mathcal{J}_1\omega^2$, describing the dependence of moments of inertia on the rotational frequency, have been adopted in the derivation of the quasiparticle alignments. It can be seen that all of the four bands have rather similar alignments over a wide range of rotational frequencies, which indicates that the high-$j$ orbitals involved in their configurations are the same. Bands 1 and 2 were previously proposed as chiral doublet bands built on the same $\pi(1g_{9/2})^{-1} \otimes \nu(1h_{11/2})^1$ configuration [14]. In band 1, there is an increase in alignment at $\hbar\omega \sim 0.54$ MeV, while in band 2 the increase in alignment occurs at $\hbar\omega \sim 0.34$ MeV. The alignment values in bands 3 and 4 are similar to each other and a bit larger than those of bands 1 and 2. The $B(M1)/B(E2)$ ratios derived in the present analysis agree with that of presented in Ref. [14] with one exception. The in-band *B(M1)/B(E2)* ratio for the $15^-$ state of band 2 is about five times larger in the present analysis than the published value. It is very large compared to the values derived for the other levels, due to the rather small intensity of the 949 keV E2 transition. This may be a sign of a configuration change in band 2 at this level.

It is seen in Fig. 3 that the new bands, similarly to the previously published ones, have quasiparticle alignment values around $8\hbar$, which shows that very probably the $\pi(1g_{9/2})^{-1} \otimes \nu(1h_{11/2})^1$ high-$j$ configuration is part of their quasiparticle configurations. Indeed, we assign the $\pi(1g_{9/2})^{-1} \otimes \nu(1g_{7/2})^{-2}(1h_{11/2})^1$ four-quasiparticle configuration to these bands based on the following discussion. This observation raises the possibility of the existence of multiple chiral doublet bands, M$\chi$D, in this nucleus, similarly to the case of $^{103}$Rh.

The standard fingerprints of chiral bands, i.e., close excitation energies, a constant staggering parameter $S(I) = [E(I) - E(I-1)]/2I$, and a similar behavior of the $B(M1)/B(E2)$ ratios of transition probabilities, are fulfilled for both the bands 1 and 2, as well as for bands 3 and 4 as seen in Fig. 5. Thus, there may be two pairs of composite chiral partners, bands 1 and 2, as well as bands 3 and 4, in $^{104}$Rh.

In order to understand the nature of the observed negative-parity band structure in $^{104}$Rh, first adiabatic and configuration-fixed constrained CDFT calculations [24] were performed to search for the possible configurations and deformations. With the obtained configurations and deformations, quantum particle rotor model [28,36,37] calculations were performed to study the energy spectra and *B(M1)/B(E2)* ratios.

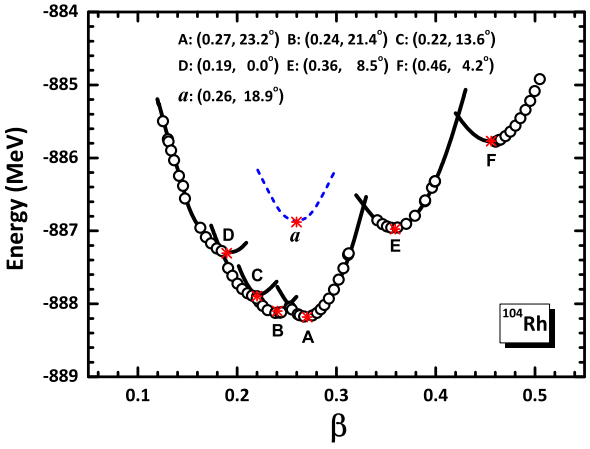


**Fig. 4.** The potential energy as a function of $\beta$ in adiabatic (open circles) and configuration-fixed (lines) constrained triaxial RMF calculations with the effective interaction PC-PK1 for $^{104}$Rh. The $\beta$ and $\gamma$ shape parameters of the labeled states are given in parentheses.

**Table 1**
The excitation energies $E_x$, deformation parameters $\beta$ and $\gamma$, and their corresponding configurations (valence nucleon and unpaired nucleon) as well as the parities of minima for states A-F and $a$ in the configuration-fixed constrained triaxial CDFT calculations.

| State | $E_x$ | $(\beta,\gamma)$ | Unpaired configuration | $\pi$ |
|---|---|---|---|---|
| A | 0.00 | (0.27, 23.2°) | $\pi(1g_{9/2})^{-1} \otimes \nu(1h_{11/2})^1$ | − |
| B | 0.08 | (0.24, 21.4°) | $\pi(1g_{9/2})^{-1} \otimes \nu(1g_{7/2})^{-1}$ | + |
| C | 0.29 | (0.22, 13.6°) | $\pi(2p_{1/2})^1 \otimes \nu(1g_{7/2})^{-1}$ | − |
| D | 0.87 | (0.19, 0.0°) | $\pi(1g_{9/2})^1 \otimes \nu(1g_{7/2})^{-1}$ | + |
| E | 1.21 | (0.36, 8.5°) | $\pi(1g_{7/2})^1 \otimes \nu(1h_{11/2})^1$ | − |
| F | 2.41 | (0.46, 4.2°) | $\pi(2p_{3/2})^{-1} \otimes \nu(1g_{9/2})^{-1}$ | − |
| $a$ | 1.30 | (0.26, 18.9°) | $\pi(1g_{9/2})^{-1} \otimes \nu(1g_{7/2})^{-2}(1h_{11/2})^1$ | − |

By minimizing the energy with respect to the deformation $\gamma$ for a given $\beta$, both adiabatic and configuration-fixed constrained triaxial CDFT calculations have been performed with the effective functional PC-PK1 [38] for $^{104}$Rh. The obtained potential energy curves (PECs) are shown in Fig. 4. The adiabatic PEC (open circles) is separated into several regions owing to different configurations and the uninterrupted PEC (lines) with a certain configuration can be derived from the corresponding configuration-fixed constrained calculations. This gives the local minima A, B, C, D, E and F in Fig. 4. The excitation energy $E_x$, deformation parameters, valence and unpaired nucleon configurations, and parity for these minima are summarized in Table 1. It is found that these minima A-F are all with two unpaired nucleon configurations. As shown in Fig. 4, the configuration-fixed constrained calculation is also performed with the four unpaired nucleon configuration $a$. Its corresponding information is also listed in Table 1.

State A is the ground state, with a triaxial deformation (0.27, 23.2°) and an unpaired nucleon configuration $\pi(1g_{9/2})^{-1} \otimes \nu(1h_{11/2})^1$. This configuration was assigned to bands 1 and 2 [14]. States B, C, D, E, and F have the unpaired nucleon configurations $\pi(1g_{9/2})^{-1} \otimes \nu(1g_{7/2})^{-1}$, $\pi(2p_{1/2})^1 \otimes \nu(1g_{7/2})^{-1}$, $\pi(1g_{9/2})^1 \otimes \nu(1g_{7/2})^{-1}$, $\pi(1g_{7/2})^1 \otimes \nu(1h_{11/2})^1$, and $\pi(2p_{3/2})^{-1} \otimes \nu(1g_{9/2})^{-1}$, respectively. Of which states B and D are positive parity states, while states C, E, and F are negative parity states. For these negative parity states, states C and F do not contain high-$j$ valence nucleon orbital, while state E has a slight triaxial deformation. In addition, one notes that the energy difference between states A and C is rather small. Currently, we have not accounted for potential admix-

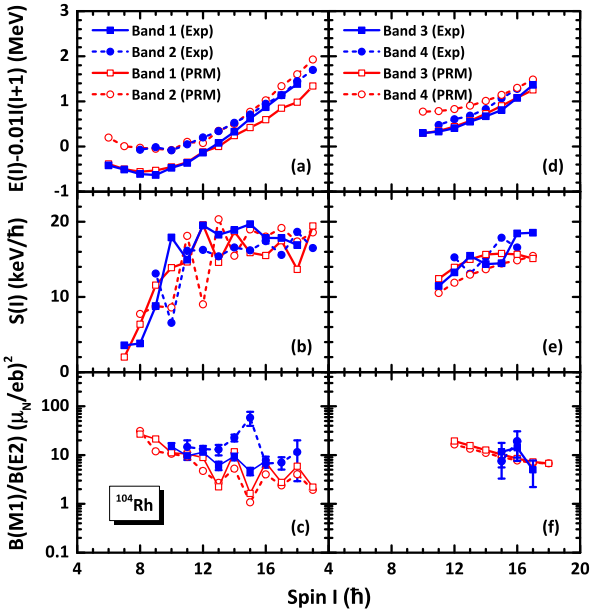


**Fig. 5.** Comparisons between the experimental and theoretical excitation energies relative to a reference rotor $E(I)-0.01I(I+1)$, $S(I)=[E(I)-E(I-1)]/2I$ parameters, and the $B(M1)/B(E2)$ ratios of transition probabilities for the doublet bands 1 and 2 (left panel) and doublet bands 3 and 4 (right panel) in $^{104}$Rh.

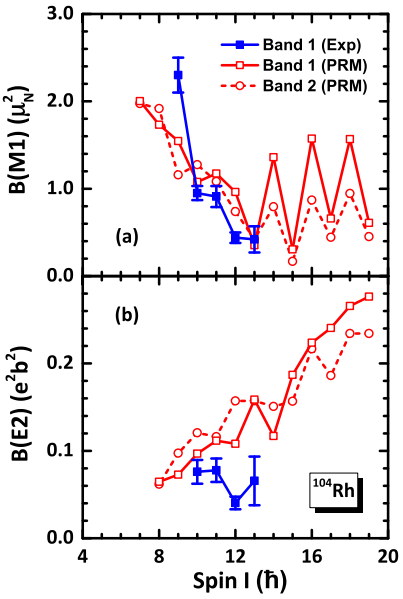


**Fig. 6.** Comparisons between the experimental and theoretical $B(M1)$ and $B(E2)$ values of transition probabilities for the doublet bands 1 and 2 in $^{104}$Rh. The experimental data is taken from Ref. [44].

tures between these states. The reason of this omission is that any such admixtures would necessitate a two-body interaction potential linking a $p_{1/2}$ and $g_{9/2}$ proton with a $\Delta l=3$, alongside a $(d_{5/2},g_{7/2})$ and $h_{11/2}$ neutron with a $\Delta l=3$ or 1. We anticipate that such admixtures would be negligible in magnitude. However, it is necessary to include these potential admixtures in further analysis for a more precise description of the bands. For the minima with four unpaired nucleons, state $a$ is a negative parity state with triaxial deformation parameter $\gamma=18.9°$, which is favorable to the chiral doublet bands. Its excitation energy with respect to the ground state is about 1.30 MeV, which is consistent with the band-head energy 1.397 MeV of band 3 at $I=10\hbar$. We assign this configuration to the bands 3 and 4.

With the obtained configurations A and $a$, and with the corresponding deformation parameters from the constrained triaxial CDFT calculations, quantum particle rotor model (PRM) [39–43] calculations were performed to study the spectroscopic properties of bands 1-4. Fig. 5 shows the experimental and theoretical excitation energies relative to a reference rotor $E(I)-0.01I(I+1)$, the staggering parameters $S(I)$, and the $B(M1)/B(E2)$ ratios for the doublet bands 1 and 2 (left panel) and for the doublet bands 3 and 4 (right panel). In the PRM calculations, the moments of inertia $\mathcal{J}_k=\mathcal{J}_0\sin^2(\gamma-2k\pi/3)$ with $\mathcal{J}_0=16\ \hbar^2$/MeV and 24 $\hbar^2$/MeV, adjusted to reproduce the trend of the energy spectra of the doublet bands, are used for the bands 1-2 and bands 3-4, respectively. For the electromagnetic transition, the empirical intrinsic quadrupole moment $Q_0=(3/\sqrt{5\pi})R_0^2Z\beta$ with $R_0=1.2A^{1/3}$ fm, gyromagnetic ratio $g_R=Z/A=0.43$, $g_\pi(g_{9/2})=1.26$, $g_\nu(h_{11/2})=-0.21$, $g_\nu(g_{7/2})=0.70$, and $g_\nu(d_{5/2})=-0.46$ are adopted. Here, the proton and neutron $g$ factors are determined from $g_{p(n)}=g_l+(g_s-g_l)/(2l+1)$ with $g_l=1(0)$ for protons (neutrons) and $g_s=0.6g_s$(free). As shown in Fig. 5, the PRM results reasonably agree with the data, which confirm the present configuration assignments.

For bands 1-2, the PRM results excellently agree with the experimental energy spectra for $I\leq 14\hbar$, and deviate from the data in the higher spin region since the configuration has changed (cf. Fig. 3). These two bands are separated by $\sim 540$ keV at $I=8\hbar$. They approach each other with increasing spin, and the separation finally goes to $\sim 200$ keV at $I=14\hbar$. The energy difference between the doublet bands is rather large since their triaxial deformation is still small to form the static chirality. As shown in Fig. 3, the theoretical alignment for band 1 shows a smooth increase rather than a sharp increase. For band 2, the theoretical alignment deviates from the data at the high rotational frequency region, which indicates that the adopted configuration becomes not appropriate. The experimental staggering parameter $S(I)$ is seen to vary smoothly with spin. The calculated $S(I)$ values for band 2 show a little staggering behavior. The $B(M1)/B(E2)$ ratios of bands 1 and 2 are similar, which further supports the interpretation in terms of chiral doublets between bands 1 and 2. The calculated $B(M1)/B(E2)$ is smaller than the experimental data. The staggering behavior is reproduced for band 1 in $I<14\hbar$. For band 2, there is no obvious staggering at $I<14\hbar$, which is also reproduced by PRM. However, the $B(M1)/B(E2)$ peak of band 2 at $I=15\hbar$ is not reproduced, which can be attributed to the band crossing.

We further compare the experimental and theoretical $B(M1)$ and $B(E2)$ transition probability values for doublet bands 1 and 2, as depicted in Fig. 6. Noting that experimental data is available only for band 1 [44]. The PRM calculations reasonably reproduce the experimental $B(M1)$ values, while they tend to overestimate the experimental $B(E2)$ values. This observation raises the possibility that the CDFT calculations may have overestimated the $\beta$ deformation parameter. Additionally, time dependent perturbed angular distribution (TDPAD) measurements have been reported for the magnetic moment of the isomeric $6^-$ band head within band 1 in Ref. [14]. The resulting $g$ factor value obtained for this state is determined to be $g=0.33(2)$. In the PRM, the $g$ factor is calculated to be $g=0.25$, a bit smaller than the experimental data. We have further checked that for this state, the rotor angular momentum components are $R_{m,s,l}=3.15$, 1.87, and $1.38\hbar$, which gives rotor angular momentum vector length $|\boldsymbol{R}|\sim 3.9\hbar$, smaller than the proton hole ($|\boldsymbol{j}_p|\sim 5\hbar$) and neutron particle ($|\boldsymbol{j}_n|\sim 6\hbar$) angular momentum vector. As seen in the following, this state shows the chiral vibration feature.

Elucidation of the chirality evolution with increasing angular momentum is provided in Fig. 7, where probability distributions for the projection onto the long ($l$), intermediate ($i$), and short ($s$) axes are presented. At spin $I=6$, 8, 10, and $12\hbar$, the $K$ distributions for bands 1 and 2 distinctly exhibit characteristics of chiral vibration. Specifically, the maximum $K_i$ distribution occurs near $K_i=0$ for band 1, and at $K_i=4$, 6, 8, and 10 for band 2, respectively. In this spin region, band 1 corresponds to the zero-phonon state, while band 2 represents the one-phonon state. Upon reaching $I=14$ and $16\hbar$, the $K$ distributions

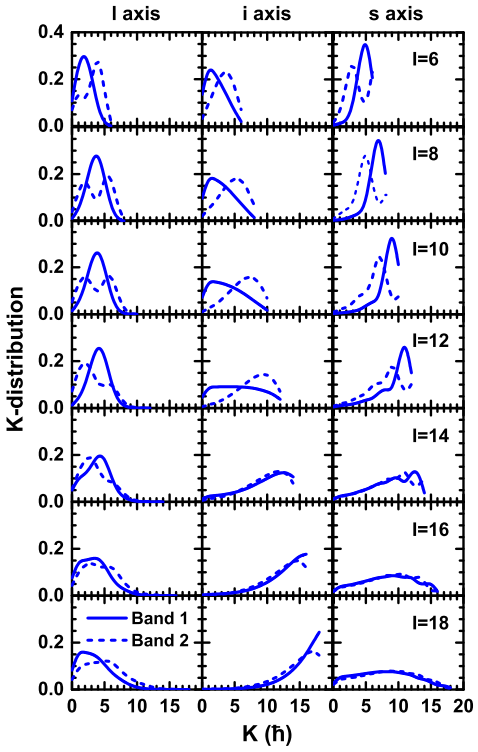


**Fig. 7.** Probability distributions for projections $K$ of total angular momentum on the long ($l$), intermediate ($i$), and short ($s$) axes for the doublet bands 1 and 2 in $^{104}$Rh.

for bands 1 and 2 become similar, demonstrating the characteristics of static chirality. The rotational mode changes from the planar to the aplanar mode, consistent with the increasing alignment shown in Fig. 3. At $I = 18\hbar$, the $K_l$ distributions for bands 1 and 2 become different. The maximum $K_l$ distribution occurs near $K_l = 0$ for band 1 and at $K_l = 6$ for band 2. This shows that the motion contains a vibration through the $i$-$s$ plane. However, one notes that the maximum $K_i$ distribution of bands 1 and 2 occurs at a large value for $I = 14$, 16, and $18\hbar$. The rotational mode tends to be principal axis rotation, resulting in the observed staggering behavior of the $B(M1)$ values, as depicted in Fig. 6.

Bands 3-4 are associated with the configuration $\pi(1g_{9/2})^{-1} \otimes \nu(1g_{7/2})^{-2}(1h_{11/2})^{1}$. The energy separation between bands 3 and 4 was found to be $\sim 200$ keV, which, combined with the spin-independent $S(I)$ parameter and the similar $B(M1)/B(E2)$, leads to the interpretation of these bands being chiral partners as well. One notes that the PRM calculations overestimate the energy splitting between the doublet bands and do not reproduce the staggering behavior of $B(M1)/B(E2)$, which might indicate that the predicted $\gamma$ value is underestimated.

To investigate the angular momentum geometries of bands 3 and 4, we have calculated the expectation values of the squared angular momentum components along the intermediate ($i$), short ($s$), and long ($l$) axes for the rotor, valence neutrons, and valence proton. The results are presented in Fig. 8. In both bands 3 and 4, the valence neutrons and proton exhibit stable components. Specifically, the neutron $g_{7/2}$ holes demonstrate minor components along the three principal axes, the neutron $h_{11/2}$ particle aligns mainly along the $s$ axis, and the proton $g_{9/2}$ hole aligns mainly along the $l$ axis. As for the collective core angular momentum, it predominantly aligns along the $s$ axis within the region of $I \leq 15\hbar$, and subsequently shows a tendency to align along the $i$ axis. Consequently, the $i$ axis component of the total angular momentum becomes comparable with the $s$ axis one around $I = 15\hbar$. As a result, the energy difference between the doublet bands becomes the smallest. Hence, the chiral vibration region is predicted for $I \leq 15\hbar$, followed by the onset of chiral rotation. However, it should be noted that the $l$ axis

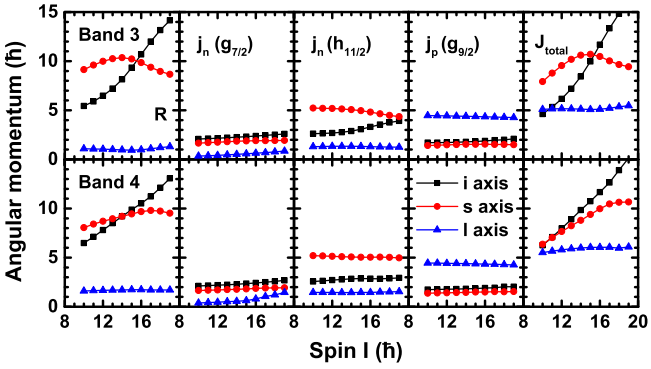


**Fig. 8.** The root mean square angular momentum components along the intermediate ($i$, squares), short ($s$, circles), and long ($l$, triangles) axes of the rotor $\boldsymbol{R}$, valence neutrons $\boldsymbol{j}_n$, valence proton $\boldsymbol{j}_p$, and total nucleus $\boldsymbol{J}_{total}$ for bands 3 (top panel) and 4 (bottom panel) calculated by PRM.

component is relatively small, and the total angular momentum closely approximates the $i$-$s$ plane.

## 4. Summary

In summary, two new negative-parity bands have been identified in $^{104}$Rh beside the already known chiral doublet structure. The observed properties of the four bands are rather similar, and the levels with the same spin-parities are close to each other in energy. To search for multiple chiral doublet bands in this nucleus, the properties of the observed bands have been compared with results of calculations involving adiabatic and configuration-fixed constrained CDFT, as well as quantum PRM calculations. According to this comparison, the lower energy parts of bands 1 and 2 form a chiral doublet structure based on the $\pi(1g_{9/2})^{-1} \otimes \nu(1h_{11/2})^{1}$ configuration, while bands 3 and 4 also form a chiral doublet based on the $\pi(1g_{9/2})^{-1} \otimes \nu(1g_{7/2})^{-2}(1h_{11/2})^{1}$ configuration. In bands 1 and 2, the chiral vibration phenomenon is predicted within the range of angular momentum values up to $12\hbar$, which is succeeded by chiral rotation occurring in the region of $13 \leq I \leq 16\hbar$. Beyond this region, the nucleus tends to orient along the $i$ axis and changes to a principal axis rotation behavior. In bands 3 and 4, the chiral vibration phenomenon is predicted to be within $I \leq 15\hbar$, followed by the onset of chiral rotation. It provides the first experimental evidence for M$\chi$D in an odd-odd nucleus in the $A \sim 100$ mass region.

## Declaration of competing interest

The authors declare that they have no known competing financial interests or personal relationships that could have appeared to influence the work reported in this paper.

## Data availability

The data that has been used is confidential.

## Acknowledgements

The crew and staff of the 88-Inch Cyclotron are thanked. Special thanks to A. O. Macchiavelli and I. Y. Lee for their help in the experiment. This work was supported by the National Research, Development and Innovation Fund of Hungary (NKFIH), financed by the project with contract No. TKP2021-NKTA-42, as well as under the K18 funding scheme with projects No. K128947 and No. K147010. This work was supported in part by the National Natural Science Foundation of China under Grant No. 12205103, the Natural Sciences and Engineering Research Council of Canada under Contract No. SAPIN/371656-2010 and the UK Engineering and Physical Sciences Research Council.

## References


[1] S. Frauendorf, J. Meng, Nucl. Phys. A 617 (1997) 131.
[2] K. Starosta, et al., Phys. Rev. Lett. 86 (2001) 971.
[3] A.A. Hecht, et al., Phys. Rev. C 63 (2001) 051302(R).
[4] D.J. Hartley, et al., Phys. Rev. C 64 (2001) 031304(R).
[5] T. Koike, K. Starosta, C.J. Chiara, D.B. Fossan, D.R. LaFosse, Phys. Rev. C 63 (2001) 061304(R).
[6] R.A. Bark, A.M. Baxter, A.P. Byrne, G.D. Dracoulis, T. Kibédi, T.R. McGoram, S.M. Mullins, Nucl. Phys. A 691 (2001) 577.
[7] K. Starosta, C.J. Chiara, D.B. Fossan, T. Koike, T.T.S. Kuo, D.R. LaFosse, S.G. Rohozinski, Ch. Droste, T. Morek, J. Srebrny, Phys. Rev. C 65 (2002) 044328.
[8] T. Koike, K. Starosta, C.J. Chiara, D.B. Fossan, D.R. LaFosse, Phys. Rev. C 67 (2003) 044319.
[9] G. Rainovski, et al., Phys. Rev. C 68 (2003) 024318.
[10] S. Zhu, et al., Phys. Rev. Lett. 91 (2003) 132501.
[11] H.C. Jain, S. Lakshmi, P.K. Joshi, AIP Conf. Proc. 764 (2005) 99.
[12] J. Srebrny, E. Grodner, T. Morek, I. Zalewska, Ch. Droste, J. Mierzejewski, A.A. Pasternak, J. Kownacki, J. Perkowski, Acta Phys. Pol. 36 (2005) 1063.
[13] E. Grodner, et al., Phys. Rev. Lett. 97 (2006) 172501.
[14] C. Vaman, D.B. Fossan, T. Koike, K. Starosta, I.Y. Lee, A.O. Macchiavelli, Phys. Rev. Lett. 92 (2004) 032501.
[15] P. Joshi, et al., Phys. Lett. B 595 (2004) 135.
[16] P. Joshi, et al., Eur. Phys. J. A 24 (2005) 23.
[17] J.A. Alcántara-Núñez, et al., Phys. Rev. C 69 (2004) 024317.
[18] J. Timár, et al., Phys. Lett. B 598 (2004) 178.
[19] J. Timár, C. Vaman, K. Starosta, D.B. Fossan, T. Koike, D. Sohler, I.Y. Lee, A.O. Macchiavelli, Phys. Rev. C 73 (2006) 011301(R).
[20] D.L. Balabanski, et al., Phys. Rev. C 70 (2004) 044305.
[21] S.Y. Wang, et al., Phys. Lett. B 703 (2011) 40.
[22] C. Liu, et al., Phys. Rev. Lett. 116 (2016) 112501.
[23] B.W. Xiong, Y.Y. Wang, At. Data Nucl. Data Tables 125 (2019) 193.
[24] J. Meng, J. Peng, S.Q. Zhang, S.-G. Zhou, Phys. Rev. C 73 (2006) 037303.
[25] J. Peng, H. Sagawa, S.Q. Zhang, J.M. Yao, Y. Zhang, J. Meng, Phys. Rev. C 77 (2008) 024309.
[26] J.M. Yao, B. Qi, S.Q. Zhang, J. Peng, S.Y. Wang, J. Meng, Phys. Rev. C 79 (2009) 067302.
[27] J. Li, S.Q. Zhang, J. Meng, Phys. Rev. C 83 (2011) 037301.
[28] A.D. Ayangeakaa, et al., Phys. Rev. Lett. 110 (2013) 172504.
[29] I. Kuti, et al., Phys. Rev. Lett. 113 (2014) 032501.
[30] C. Petrache, et al., Phys. Rev. C 97 (2018) 041304(R).
[31] I.Y. Lee, Nucl. Phys. A 520 (1990) 641c.
[32] R.V.F. Janssens, F.S. Stephens, Nucl. Phys. News 6 (1996) 9.
[33] D.C. Radford, Nucl. Instrum. Methods A 361 (1995) 297;
D.C. Radford, Nucl. Instrum. Methods A 361 (1995) 306, http://radware.phy.ornl.gov.
[34] A. Krämer-Flecken, T. Morek, R.M. Lieder, W. Gast, G. Hebbinghaus, H.M. Jäger, W. Urban, Nucl. Instrum. Methods A 275 (1989) 333;
K.S. Krane, R.M. Steffen, R.M. Wheeler, Nucl. Data Tables A 11 (1973) 351.
[35] R. Bengtsson, S. Frauendorf, Nucl. Phys. A 327 (1979) 139.
[36] B. Qi, S.Q. Zhang, J. Meng, S.Y. Wang, S. Frauendorf, Phys. Lett. B 675 (2009) 175.
[37] B. Qi, S.Q. Zhang, S.Y. Wang, J. Meng, T. Koike, Phys. Rev. C 83 (2011) 034303.
[38] P.W. Zhao, Z.P. Li, J.M. Yao, J. Meng, Phys. Rev. C 82 (2010) 054319.
[39] Q.B. Chen, K. Starosta, T. Koike, Phys. Rev. C 97 (2018) 041303(R).
[40] Q.B. Chen, J. Meng, Phys. Rev. C 98 (2018) 031303(R).
[41] Q.B. Chen, B.F. Lv, C.M. Petrache, J. Meng, Phys. Lett. B 782 (2018) 744.
[42] Q.B. Chen, N. Kaiser, U.-G. Meissner, J. Meng, Phys. Rev. C 99 (2019) 064326.
[43] Q.B. Chen, N. Kaiser, U.-G. Meissner, J. Meng, Phys. Lett. B 807 (2020) 135568.
[44] T. Suzuki, et al., Phys. Rev. C 78 (2008) 031302(R).